Published in final edited form as:
Science. 2013 March 22; 339(6126): 1433–1436. doi:10.1126/science.1233920.

Dynamin-driven membrane fission reveals catalytic principle of membrane remodeling

Anna V. Shnyrova[1,†], **Pavel V. Bashkirov**[2,†], **Sergey A. Akimov**[2], **Thomas J. Pucadyil**[3], **Joshua Zimmerberg**[4], **Sandra L. Schmid**[5], and **Vadim A. Frolov**[1,6,*]

[1]Biophysics Unit (CSIC-UPV/EHU) and Department of Biochemistry and Molecular Biology, University of the Basque Country, Leioa, Spain

[2]A.N. Frumkin Institute of Physical Chemistry and Electrochemistry, Russian Academy of Sciences, Moscow 119991, Russia

[3]Indian Institute of Science Education and Research (IISER), Pune, India

[4]Program in Physical Biology, Eunice Kennedy Shriver National Institute of Child Health and Human Development, National Institutes of Health, Bethesda, MD 20892, USA

[5]Department of Cell Biology, UT Southwestern Medical Center, Dallas, TX, USA

[6]IKERBASQUE, Basque Foundation for Science, Bilbao, Spain

Abstract

Biological membrane fission is conducted by protein-driven stress. To create such membrane stress the GTPase dynamin-1, protein orchestrating membrane fission in endocytosis, assembles into helical scaffolds that constrict the necks of endocytic vesicles. We found that under constant GTP turnover two-rung dynamin scaffold is sufficient to produce fission of lipid nanotubes. Analyzing membrane fission by short dynamin scaffolds, we reveal a catalytic cycle which translates constriction stresses into fission. Upon constriction, coordinated membrane wedging by the scaffold facilitates reversible merger of the inner leaflet of the nanotube, the hemifission. Modeling of this reversible step identifies a low-energy path based on geometric coupling of the scaffold and the membrane. The final translation of the metastable hemifission into complete fission is stochastically linked to disassembly of the scaffold. This catalytic conversion of localized stresses into membrane remodeling suggests a novel paradigm for fission and fusion of cellular membranes.

Main Text

Cellular membranes can merge (fusion) or split apart (fission) without compromising their barrier function. This property is based upon lipid polymorphism allowing lipids to form transient non-bilayer structures locally bridging cellular membranes at the initiation of topological transition (1–4). These connections provide a unique path for sequential remodeling of the lipid bilayer, monolayer by monolayer, thus avoiding formation of transmembrane pores and content leakage (1). In structurally stable lipid bilayers formation of non-bilayer connections requires application of membrane stress (5, 6). It follows that specialized protein complexes controlling membrane fusion and fission in cells are needed to apply membrane stress to acutely destabilize lipid bilayers. Such complexes are usually highly transient structures consisting of only a few protein molecules (7, 8). It remains an

*Correspondence to: vadim_frolov@ehu.es.
†These authors contributed equally to this work

open question whether they can rely only on pure force to ensure completion of the topological transformation within their lifetime.

This question is exemplified in the mechanism of action of dynamin-1, the paradigmatic member of the superfamily of dynamin-like GTPases involved in membrane fusion and fission (9–11). Dynamin polymerizes into helical collars constricting the necks of endocytic vesicles (9). Polymerization triggers cooperative GTP hydrolysis potentially liberating huge (100s of k_BT) amounts of energy per turn of the dynamin helix. Structural analysis of long dynamin helices indicates several possible conformational changes and/or remodeling modes capable of converting the GTP energy into a power-stroke producing acute membrane stress and fission (12–16). However, both *in vivo* and *in vitro*, dynamin appears to operate in small units (6, 8, 17), and it remains unclear how much of the energy generated through polymerization of a small dynamin complex and subsequent GTP hydrolysis is converted into local deformations of the lipid bilayer.

To quantify the efficiency of the dynamin fission machinery, we reconstituted activity of the wild type (WT) dynamin-1 (further dynamin) on lipid nanotubes (NTs). The dramatic constriction upon dynamin polymerization on long NTs (pulled from Giant Unilamellar Vesicles (GUV) or SUPER templates (18, 19)) was observed as a decrease of NT membrane and lumenal fluorescence at the places where the dynamin scaffold forms (Fig. 1A, B). The coincidence of axial profiles of fluorescence intensity coming from both a membrane-incorporated lipid label (Rh-DOPE) and a lumenal aqueous dye (3kDa dextran) (Fig. 1B) indicates that the lipid label correctly reports membrane constriction. Histograms of membrane fluorescence intensities reporting the NT diameter display two populations (corresponding to the bare and constricted NT regions) which are similarly distributed with or without GTP (Fig. 1F). Thus, the average membrane curvature imposed by the scaffolds does not appear to depend on the presence of the nucleotide, and instead is driven mainly by dynamin polymerization (6, 17). In the absence of GTP or under conditions favoring membrane binding of dynamin, multiple long dynamin scaffolds develop. The scaffolds grow independently until they cover a substantial part of the NT, so that the membrane deformations produced by individual scaffolds start interfering with each other (Fig. 1C, Movie S2). This interference results in membrane bulging (Fig. 1C), which prevents merger of the neighboring scaffolds (20) and stalls their growth. In the absence of GTP, these dynamin scaffolds remain virtually static (Fig. 1D, E). However, in the presence of 1 mM GTP, NT constriction reaches a quasi steady-state situation (Fig. 1C) during which GTP hydrolysis fuels large fluctuations of the length of *individual* scaffolds (Fig. 1D, E, S1; Movies S2, S3). This reflects GTPase-driven cycles of disassembly (frequently almost complete, as indicated by the tail in the histogram in Fig. 1E, lower panel) and reassembly of the scaffolds before membrane fission (6, 13, 17, 21). Together, these observations indicate that the energy released by GTP hydrolysis causes softening (“melting”) of the dynamin polymer, rendering it metastable.

Analysis of scaffold disassembly dynamics post fission suggests that external forces, including those related to membrane tensile stress, can accelerate disassembly of the dynamin scaffolds formed in the presence GTP. A single fission event on NTs pulled from GUVs under tension, results in rapid disassembly of the entire scaffold and concomitant retraction of the tubule (Fig. 1G, H, Movie S4); whereas free floating membranes remain tubular and stochastically break into numerous pieces (17) (Movie S5). In contrast, in the absence of GTP, dynamin assemblies can withstand membrane tension (Fig. 1I, Movie S6). This force sensitivity further corroborates the metastable character of the long dynamin scaffolds in the presence of GTP and also indicates that the metastability is directly linked to fission. The question remains whether this link is relevant for the membrane fission produced by much shorter dynamin complexes assembling under physiological conditions.

To observe dynamin activity at nanoscale we measured the ionic permeability (conductance) of short (submicron) NTs pulled from a planar lipid bilayer (6). In the absence of GTP, the constriction starts from a rapid nucleation of short dynamin scaffolds (22). The scaffolds then grow either monotonically (Fig. 2A) or in a stepwise manner (Fig. 2B). Similar patterns of membrane-constriction activity are detected by fluorescence measurements on long NTs (Fig. S1), confirming that the conductance decrease reports NT constriction. The refractory period before the steps likely reflects a slow disappearance of a membrane bulge between the neighbor scaffolds followed by merger of the scaffolds (Fig. S1B). Independent of the pathway and the NT length, the final steady-state conductance is always close to the value characteristic for a uniformly squeezed NT of fixed lumenal diameter (~5 nm, $2R_{Dyn}$, Fig. 2A), as expected (6). Given the bimodal distribution of constricted and bare tubules (Fig. 1F), the change in conductivity (ΔG_n) can be used to estimate the length (L_S) of the constricted region upon each constriction step (Fig. 2D, left panel).

In the presence of GTP, dynamin effectively severs short NTs (80 to 2000 nm in length) directly demonstrating that very short dynamin scaffolds are sufficient to produce fission *in vitro*. Fission follows a period of wave-like conductance behavior (Fig. 2C, upper graph, also see (6)), indicating cycles of assembly/disassembly of the protein scaffold upon GTP hydrolysis. Corroborating this notion, at lower concentrations of GTP, the disassembly prior to fission is slower (upper versus lower graph in Fig. 2C). We did not observe a single example of a rapid ~2-fold conductance decrease which would correspond to a concerted GTP-dependent increase in constriction or extension of a short dynamin scaffold (12, 13, 23). Rather, our data demonstrate slow, iterative cycles of membrane constriction resembling a stochastic optimization process (6).

Assuming that a dynamin scaffold in the presence of GTP imposes the same local curvature as without GTP (as indicated by Fig. 1E,F), we can derive the length of the dynamin scaffolds from conductance changes (Fig 2D, right panel). Such analysis demonstrates that the scaffolds producing the conductance waves (Fig. 2E, +GTP curve) are substantially shorter than the scaffolds producing conductance steps in the absence of GTP (Fig. 2E -GTP curve). Even shorter, 20–50 nm dynamin scaffolds, produce fission, as indicated by the shift in the distribution of the scaffold length (from +GTP to “fission” curves, Fig. 2E). Hence, the metastability of the dynamin scaffolds under constant GTP turnover, seen in fluctuation of the scaffold length (Fig 1D, E, Fig. 2C), allows to optimize the scaffold length to produce fission.

The smallest constriction steps detected upon dynamin polymerization without GTP were close to ΔL~20nm (Fig. 2E, insert), well above than the noise level in our measurements (Fig. 2D). This length approximately corresponds to two rungs of a dynamin helix with a pitch of ~10nm (9), indicating that curvature nucleation requires at least a two-rung scaffold. The length of the shortest constriction detected prior to fission (Fig. 2E, insert) also corresponds to the two-rung dynamin helix, the minimal unit required to form a complete ring of activated GTPase domain dimers (24). Thus, a two-rung dynamin complex constitutes the minimal dynamin machinery producing membrane curvature and fission.

In ~ 10% of trials we found that the acute loss of conductance, indicative of closure of the NT lumen, is followed by its restoration (Fig. 2F), reminiscent of the flickering conductance of fusion and fission pores measured in cellular systems (25–29). As *in vivo*, the NT conductance switches between “open” and “closed” states. It stays in the “closed” state for tens of ms, which is much longer that the characteristic time of the transition between the two states (<1 ms), indicating a metastable intermediate. Two observations indicate that this closed state corresponds to a hemifission-type structure (1, 4, 6). First, we never (0/24 fission events recorded using short NTs) detected a sharp conductance increase

characteristic of content leakage, implying that a hemifission intermediate precedes complete fission (1, 6). Second, because complete fission in our system triggers the rapid disassembly of metastable dynamin scaffolds (Fig. 1G, H), it is unlikely that the flicker reflects a cycle of fission and fusion. Hence, the flicker of the NT conductance reveals spontaneous transitions between the two main intermediates of membrane fission: a constricted tube (resembling the constricted neck of a transport vesicle (25)) and hemifission. We speculate that the flicker phenomenon in membrane fusion, which reflects a similar transformation between a narrow fusion pore and hemi-fusion intermediate, may also be mediated by a ring-like protein complex.

The characteristic time for flicker (10s of milliseconds, Fig. 2F) is much smaller than the characteristic time for reassembly of the dynamin polymer (seconds, Fig. 2C). Furthermore, the “open” state is characterized by a preset conductance level (Fig. 2F, red line), indicating that the flickering NT is supported by a dynamin scaffold of fixed geometry. Such scaffolds maintain the same curvature as those formed in the absence of GTP (Fig. 1F), but here no flicker was detected. Thus, the GTP hydrolysis produces a metastable transition state (“soft” scaffold) between fully assembled (no GTP) and disassembled (GDP-bound (13, 21)) scaffolds. Previously, we proposed that fully assembled scaffolds bring membrane curvature to a critical point sufficient to trigger spontaneous fission (6). This constricted state, however, is stabilized by the same scaffold producing constriction so that fission requires GTP-dependent disassembly of the scaffold (6). Now we reveal that the scaffold, still in the constricted state, can mediate half of the topological transition, up to the hemifission intermediate, during GTP hydrolysis. Given that hemifission is reversible and is not linked to any additional curvature stress, the scaffold acts, by definition, as a catalytic center that orchestrates topological membrane transitions. That is, it “recognizes” and transiently stabilizes the local constricted and the hemifission states and provides a two-way low energy path between them (30, 31). Conversion of hemifission into complete fission is linked to tension-enhanced disassembly of this short dynamin scaffold (Fig. 1H), thus completing the fission cycle.

We next explored the molecular basis for the catalytic activity of short dynamin scaffolds, focusing on the hydrophobic membrane-inserting variable loop 1 (VL1) of Pleckstrin Homology Domain (PHD) of dynamin, which provides the critical functional links between dynamin and lipids (9, 32) . We examined the activity of the I533A mutation in VL1 that reduces its hydrophobic bulk and severely inhibits the membrane fission activity of dynamin (32). I533A constricts NTs pulled from planar lipid bilayers to the same final curvature as wild type dynamin (Fig. 3A, D) producing a similar stepwise decrease in the conductance seen on submicron NTs (Fig. 3B). Moreover, in the presence of nucleotide, I533A produces conductance fluctuations closely resembling the phenotype observed with wild type dynamin (Fig. 3B, C). These data demonstrate that I533A effectively couples GTP hydrolysis to periodic curvature generation. Nonetheless, the fission activity of I533A is significantly impaired (Fig. 3A, B): it broke only 1 out of 8 short NTs, compared to 24 out of 25 for the wild type protein, and no conductance flicker was detected.

Interestingly, the fission activity of I533A on NTs pulled from SUPER templates and GUV can be restored by increasing the PI(4,5)P2 levels in the membrane (Fig. 3E, Movie S7). However, given that I533A is severely defective in clathrin-mediated endocytosis in cells (32), the lower PI(4,5)P2 conditions more accurately reflect its activity under physiological conditions. At these PI(4,5)P2 levels (1 or 2 mol%), I533A fails to produce membrane fission of the tubes pulled from either GUVs (Fig. 3F; Movies S5, S8, S9) or SUPER templates (Fig. S2). From these data, we conclude that membrane wedging by PHDs and PI(4,5)P2-dependent electrostatic adhesion between PHDs and lipids act synergistically during hemifission catalysis.

To understand this novel role of the PHD, we analyzed the membrane wedging activity of short dynamin scaffolds theoretically. Our experimental observations indicate that dynamin uses the energy of GTP hydrolysis, in part, to optimize the scaffold geometry for the hemifission catalysis. We therefore used this experimentally-determined two-ring approximation of the optimal fission machinery for our modeling. In the axial section of the nanotube the rings are seen as T-shape dynamin dimers (9) (Fig. 4A, stage 2). The membrane-interacting interface thus consists of two PHDs forming a 4.6 nm wide by 4.2 nm long pedestal oriented along the NT axis (Fig. 4B, Fig. S3). This pedestal tightly binds to the lipid bilayer through PI(4,5)P2-dependent electrostatic interactions and also drives a pronounced hydrophobic wedge into the NT membrane (9, 21) (Fig. 4B). The cylindrical membrane of a constricted NT has zero azimuthal curvature while that of the hemifission intermediate is substantially negative (Fig. 4A, stage 2 and 4 (6, 33)). Thus, we argue that in order to minimize membrane stresses PHDs must tilt with progression of membrane deformations towards hemifission (Fig. 4A, tilt angle α). Indeed PHDs are flexibly linked to the rest of the dymanin dimer (14–16) and the bridging of the rings during GTP hydrolysis (24) shall further facilitate tilting (Fig. 4A). Our calculations (described in details in Supplementary online text) demonstrate that if we fix the width of the wedge to a reasonable value (0.7 nm) and allow PHDs to optimize the tilt angle, the resulting energy barrier decreases dramatically to several k_BT (Fig. 4C). This means that if, in the GTP-dependent metastable state, dynamin scaffolds can simply follow membrane deformations by changing the tilt angle (Fig. S5), then the topological transition becomes spontaneous.

The tilt angle can be changed constantly to minimize the elastic stresses at each point of the topological transition. Alternatively, PHDs could adopt a fixed tilt. At zero tilt (Fig. 4A, stage 2), the energy barrier remains high (Fig 4C, red curve), indicating that pure constriction is ineffective in producing fission (6, 33). At non-zero constant tilt, dynamin scaffold produces torque. We found, however, that for the same insertion width (0.7nm here) the decrease of the energy barrier produced by torque (Fig. 4C, red line) is never more effective than that achieved by explicit coupling of the tilt angle to the membrane shape (Fig. 4C, dashed line). Both, tighter membrane adhesion of PHDs mediated by PI(4,5)P2 and widening of the effective membrane wedge enforce this local coupling between dynamin scaffold and lipids (Fig. 4C, black curve), explaining the PI(4,5)P2-mediated rescue of the fission activity of I533A (Fig. 3E). This link between the geometry of the protein scaffold, concerted membrane wedging and the shape of the lipid bilayer constitutes the essence of the hemifission catalysis.

Why the need for a catalytic stage? It is generally accepted that topological membrane remodeling (fusion and fission) requires application of stress to locally breach the integrity of the lipid bilayer. If stress is created by curvature-driven protein complexes, they generally tend to stabilize highly curved membrane structures thereby effectively inhibiting topological transitions (34), just as tighter substrate binding inhibits enzymatic catalysis (31). Hence our findings solve this paradox: Protein complexes driving membrane fission combine membrane curvature activity with specific structural flexibilities allowing for catalysis of topological remodeling (Fig. 4A). Furthermore, to ensure the completion of remodeling within the short life span of the complex, the protein and lipid rearrangements must be synchronized, e.g. via explicit catalytic feedbacks between the protein complex and the lipid matrix. Taken together, our results provide a new rationale for understanding the mechanisms of protein-driven membrane remodeling exemplified in the functional design of the dynamin machinery.

Supplementary Material

Refer to Web version on PubMed Central for supplementary material.

Acknowledgments

This work was supported in part by the Intramural Program of the NICHD and in part by the Russian Foundation for Basic Researcher (projects #11-04-01001 and #11-04-02087), Program of Presidium of RAS ‘‘Molecular and Cell Biology’’ and Federal Task Program ‘‘Scientific and Scientific-Pedagogic Personnel of Innovative Russia’’ for 2009–2013 (state contracts #P337 and #14.740.11.1409). SLS is supported by NIH grant GM42455.

We are grateful to Piotr Kuzmin for the critical discussion of the manuscript.

References and Notes

1. Frolov VA, Zimmerberg J. FEBS Lett. 2010 May 3.584:1824. [PubMed: 20100479]
2. Kozlov MM, McMahon HT, Chernomordik LV. Trends Biochem Sci. 2010 Dec.35:699. [PubMed: 20638285]
3. Leikin SL, Kozlov MM, Chernomordik LV, Markin VS, Chizmadzhev YA. J Theor Biol. 1987 Dec 21.129:411. [PubMed: 3455469]
4. Frolov VA, Shnyrova AV, Zimmerberg J. Cold Spring Harb Perspect Biol. 2011 Nov.3:a004747. [PubMed: 21646378]
5. Yang L, Huang HW. Science. 2002 Sep 13.297:1877. [PubMed: 12228719]
6. Bashkirov PV, et al. Cell. 2008 Dec 26.135:1276. [PubMed: 19084269]
7. Mohrmann R, Sorensen JB. J Mol Neurosci. 2012 Mar 17.
8. Mattheyses AL, Atkinson CE, Simon SM. Traffic. 2011 Oct.12:1394. [PubMed: 21689254]
9. Schmid SL, Frolov VA. Annu Rev Cell Dev Biol. 2011 Nov 10.27:79. [PubMed: 21599493]
10. Praefcke GJ, McMahon HT. Nat Rev Mol Cell Biol. 2004 Feb.5:133. [PubMed: 15040446]
11. Ferguson SM, De Camilli P. Nat Rev Mol Cell Biol. 2012 Feb.13:75. [PubMed: 22233676]
12. Chen YJ, Zhang P, Egelman EH, Hinshaw JE. Nat Struct Mol Biol. 2004 Jun.11:574. [PubMed: 15133500]
13. Stowell MH, Marks B, Wigge P, McMahon HT. Nat Cell Biol. 1999 May.1:27. [PubMed: 10559860]
14. Faelber K, et al. Nature. 2011 Sep 29.477:556. [PubMed: 21927000]
15. Ford MG, Jenni S, Nunnari J. Nature. 2011 Sep 29.477:561. [PubMed: 21927001]
16. Chappie JS, et al. Cell. 2011 Sep 30.147:209. [PubMed: 21962517]
17. Pucadyil TJ, Schmid SL. Cell. 2008 Dec 26.135:1263. [PubMed: 19084268]
18. Materials and methods are available as supplementary material on Science Online.
19. Pucadyil TJ, Schmid SL. Biophys J. 2010 Jul 21.99:517. [PubMed: 20643070]
20. Shlomovitz R, Gov N, Roux A. New Journal of Physics. 2011; 13:065008.
21. Ramachandran R, Schmid SL. Embo J. 2008 Jan 9.27:27. [PubMed: 18079695]
22. Roux A, et al. Proc Natl Acad Sci U S A. 2010 Mar 2.107:4141. [PubMed: 20160074]
23. Kozlov MM. Biophys J. 1999 Jul.77:604. [PubMed: 10388785]
24. Chappie JS, Acharya S, Leonard M, Schmid SL, Dyda F. Nature. 2010 May 27.465:435. [PubMed: 20428113]
25. Frolov VA, Lizunov VA, Dunina-Barkovskaya AY, Samsonov AV, Zimmerberg J. Proc Natl Acad Sci U S A. 2003 Jul 22.100:8698. [PubMed: 12857952]
26. Breckenridge LJ, Almers W. Proc Natl Acad Sci U S A. 1987 Apr.84:1945. [PubMed: 3470768]
27. He L, Wu XS, Mohan R, Wu LG. Nature. 2006 Nov 2.444:102. [PubMed: 17065984]
28. Suss-Toby E, Zimmerberg J, Ward GE. Proc Natl Acad Sci U S A. 1996 Aug 6.93:8413. [PubMed: 8710885]
29. Zimmerberg J, Curran M, Cohen FS, Brodwick M. Proc Natl Acad Sci U S A. 1987 Mar.84:1585. [PubMed: 3470745]
30. Mitchell P. Eur J Biochem. 1979 Mar 15.95:1. [PubMed: 378655]
31. Williams IH. Beilstein J Org Chem. 2010; 6:1026. [PubMed: 21085499]
32. Ramachandran R, et al. Mol Biol Cell. 2009 Nov.20:4630. [PubMed: 19776347]

33. Kozlovsky Y, Kozlov MM. Biophys J. 2003 Jul.85:85. [PubMed: 12829467]
34. Boucrot E, et al. Cell. 2012 Mar 30.149:124. [PubMed: 22464325]
35. Edelstein A, Amodaj N, Hoover K, Vale R, Stuurman N. Chapter 14. Curr Protoc Mol Biol. 2010 Oct.Unit14:20. [PubMed: 20890901]
36. Schneider CA, Rasband WS, Eliceiri KW. Nature Methods. 2012 Jun.9:671–675. [PubMed: 22930834]
37. Kuzmin PI, Akimov SA, Chizmadzhev YA, Zimmerberg J, Cohen FS. Biophys J. 2005 Feb. 88:1120. [PubMed: 15542550]
38. Hamm M, Kozlov MM. Eur. Phys. J. E. 2000; 3:323.
39. Leikin S, Kozlov MM, Fuller NL, Rand RP. Biophys J. 1996 Nov.71:2623. [PubMed: 8913600]
40. Zemel A, Fattal DR, Ben-Shaul A. Biophys J. 2003 Apr.84:2242. [PubMed: 12668433]
41. Marcelja S. Biochim Biophys Acta. 1976 Nov 11.455:1. [PubMed: 990322]

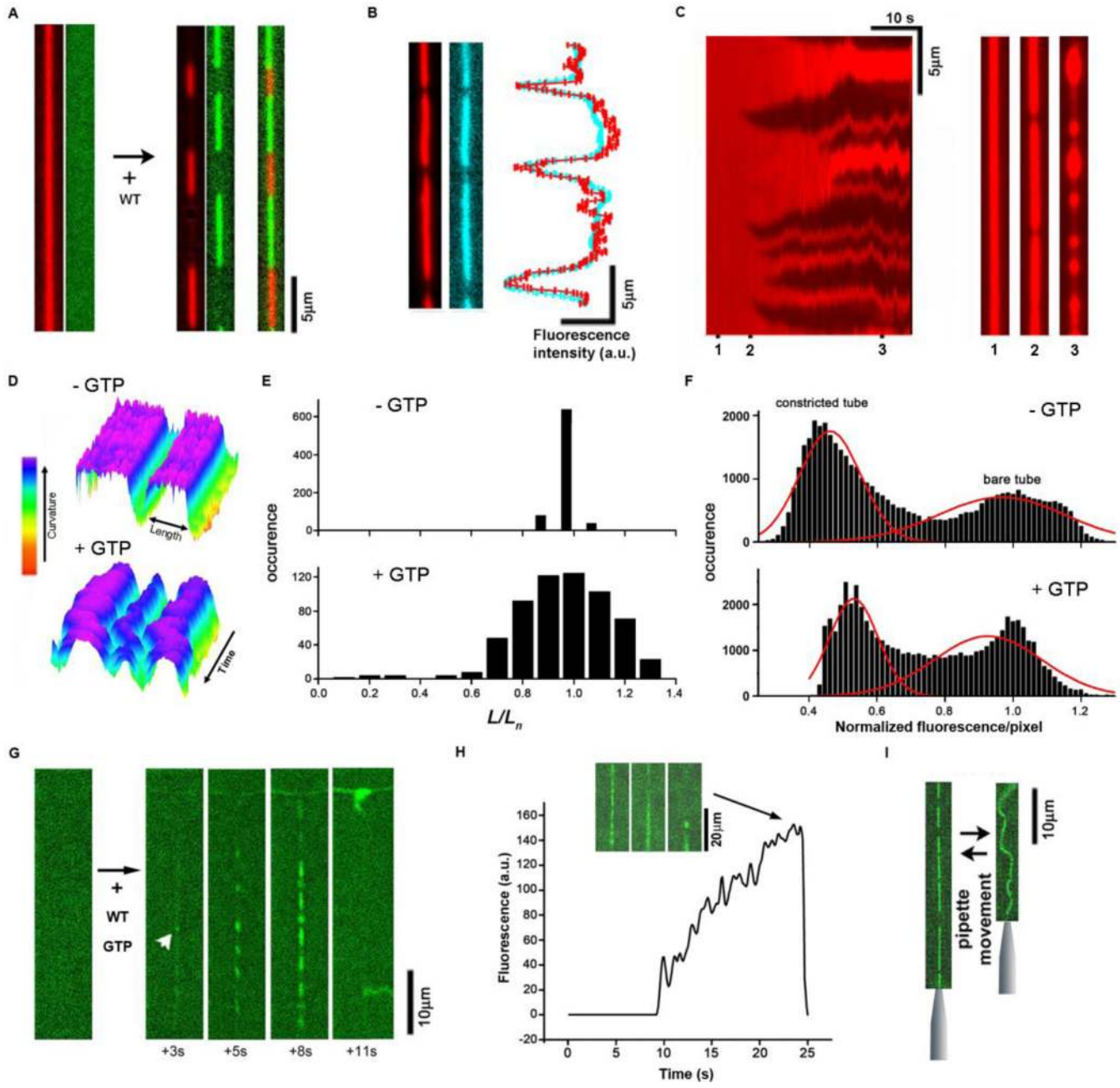

Fig. 1.

Metastable scaffolds formed by wild type dynamin (WT) under conditions of constant GTP turnover. **A.** In the absence of GTP, dynamin polymers (dyn-Alexa488 fluorescence, green) constrict lipid nanotubes (Rh-DOPE fluorescence, red). **B.** Membrane (red) and lumenal (3kDa dextran fluorescein, blue) markers show similar axial profiles marking constricted zones. **C.** Kymograph showing development of the dynamin scaffolds (dark regions) constricting lipid NT in the presence of 1 mM GTP. The selected profiles (1–3) illustrate formation of initial isolated scaffolds (2) and membrane bulging at high protein coverage (3). **D.** Kymographs showing the steady-state constriction of the NT without and with GTP as indicated. The variable lengths (*L*) of the constricted parts (blue-violet) is measured as shown. **E.** Variability of the length (*L*, see D) of constricted parts (normalized to mean

length for each scaffold (L_n)) in the steady-state. **F.** Distribution of pixel intensities for kymographs showing the development of NT constriction by dynamin (as in C). Two peaks, corresponding to bare and constricted parts, are detected both in the absence and presence of GTP. **G, H.** Rapid disassembly of the dynamin scaffold (green) upon fission, the frame sequence and the graph illustrate nucleation (white arrowhead) followed by slow accumulation and fast disappearance of the dyn-Alexa488 fluorescence in the NT (pulled from a GUV seen above) region. The insert shows images illustrating the moment of fission (100ms between frames). **I.** Without GTP the dynamin scaffold prevents shortening of the NT when a pipette holding the NT end approaches the GUV.

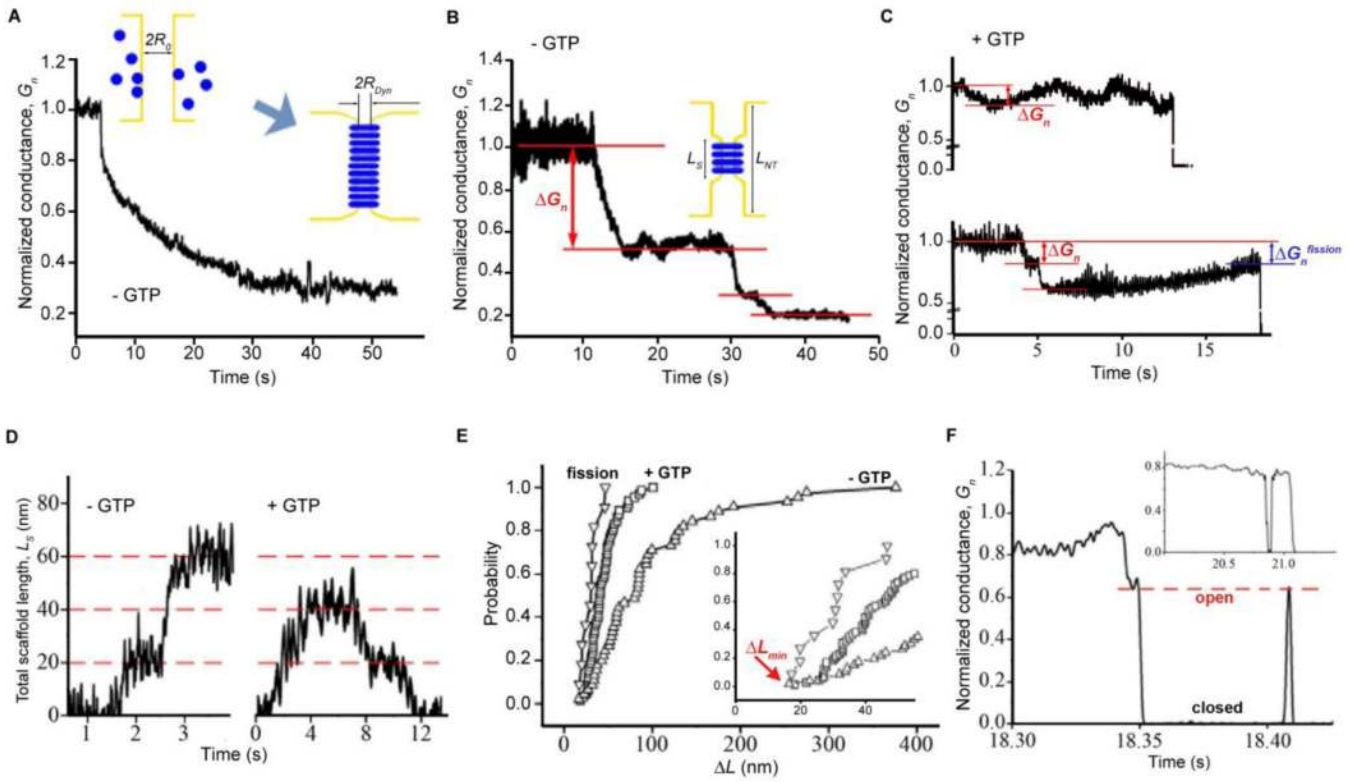

Fig. 2.

Short metastable dynamin scaffolds catalyze hemifission. **A-C.** Patterns of slow NT constriction (monotonic (A), stepwise (B) and reversible (C)) are observed by measuring the conductance of lipid NTs. Conductance is normalized to the value prior to dynamin addition. The cartoons in **A** and **B** illustrate the growth of the dynamin scaffold on NT; the initial (R_0) and the final (R_{Dyn}) radii of the nanotube are determined from the NT conductance using Ohm's law, assuming that at the final stage NT is uniformly covered by dynamin; the length of the dynamin scaffold in the intervening states (L_s) is determined from changes in G_n assuming that each scaffold constricts NT to the same radius R_{dyn}. Lower (0.2 mM GTP) and upper (1 mM GTP) panels in **C** show that GTP accelerates disassembly of the dynamin scaffold. **D.** Characteristic examples of the L_s behavior without (left) and with (right) GTP. **E.** Cumulative distribution functions of the length of the dynamin scaffold recalculated from the conductance steps (ΔG_n) measured as shown in B (- GTP, red arrow) and C (+ GTP, red arrows). Fission corresponds to the conductance of the NT prior to fission as shown in C ($\Delta G_n^{fission}$, blue arrow). The insert shows the beginning of the main graph. **F.** Reversible changes of the NT conductance ("flicker") preceding complete fission, red line illustrates the "open" state; insert shows an example of the short-living "closed" state.

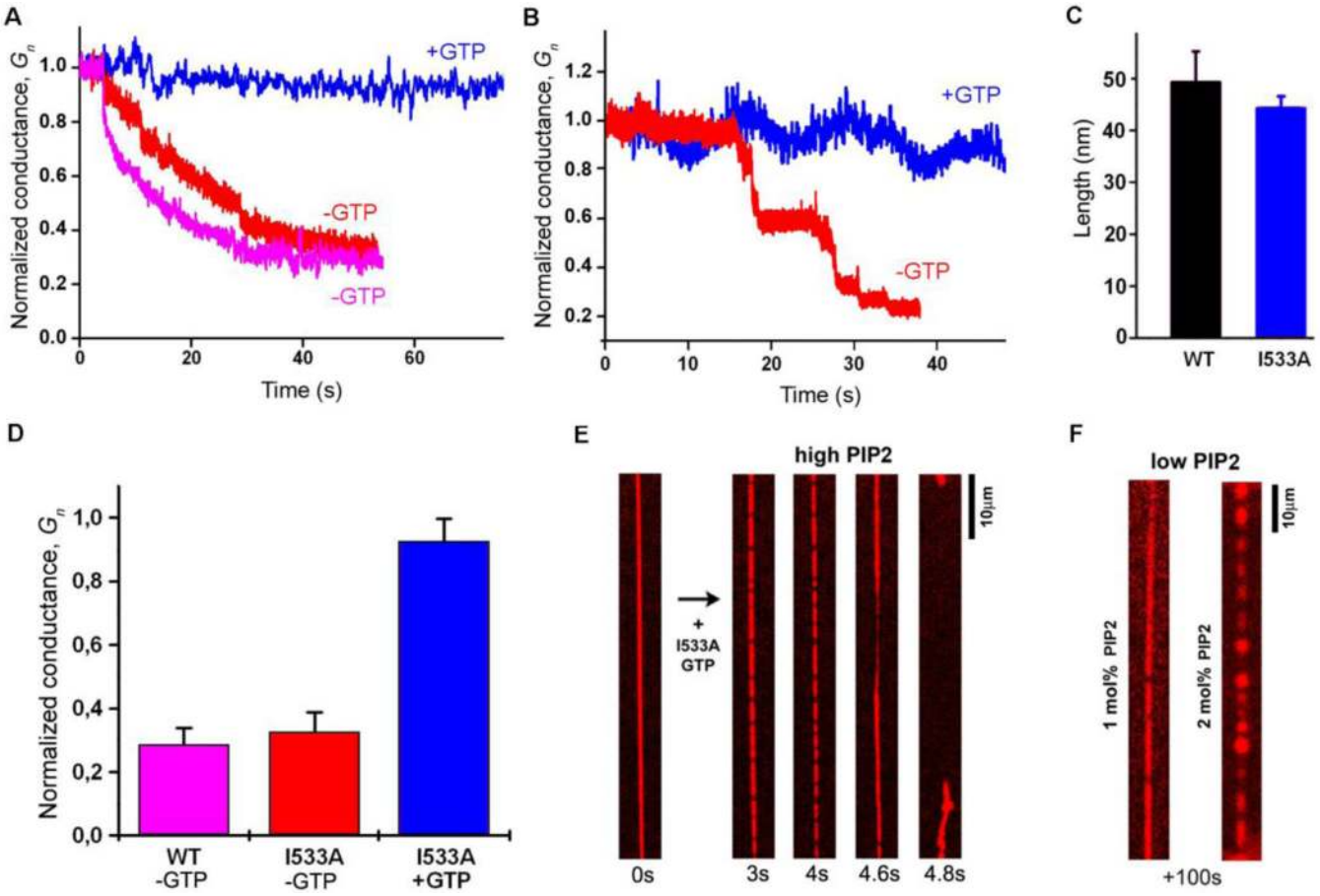

Fig. 3.

Membrane wedging plays a critical role in the hemifission catalysis. **A.** Constriction of a long NT, seen as a decrease in conductance (G_n, normalized to the value prior to dynamin addition) by WT dynamin (pink), I533A dynamin (red) and I533A in the presence of GTP (blue). **B.** The behavior of G_n upon I533A addition to short NTs with (blue) and without (red) GTP. **C.** The mean length of protein scaffolds formed by WT (black) and I533A (blue) dynamin in the presence of GTP is similar (the length is measured from ΔG_n as in Fig. 2G). **D.** Stationary NT constriction (measured in G_n units) produced by WT and I533A dynamin under conditions indicated. **E.** Frame sequence illustrating constriction and fission of NT pulled from a GUV by I533A, with 5mol% PI(4, 5)P2. Membrane fission occurs within 20s (3 trials, (32)), while at lower PIP2 concentrations (**F**) tubes remain stable at 100s time scale (1mol%PIP2 n=10, 2mol%PIP2 n=4).

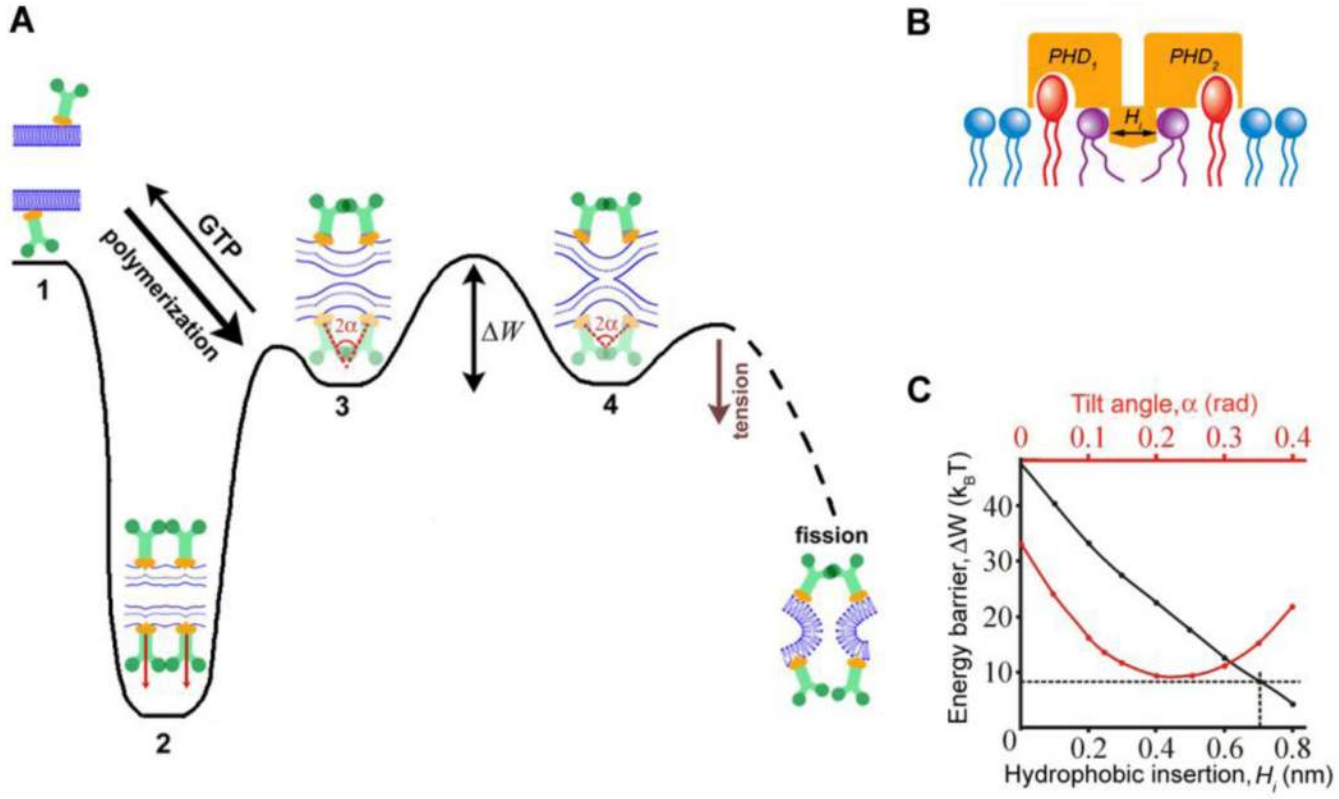

Fig. 4.

Role of membrane wedging by pleckstrin homology domain (PHD) of dynamin in the catalysis of fission. **A.** Energy diagram for dynamin-lipid complex illustrating the hemifission catalysis. Dynamin polymerization leads to formation of a highly stressed "reactant" state (2) that remains stable in the absence of GTP. GTP hydrolysis causes partial "melting" of dynamin rings resulting in a new metastable intermediate around the constricted neck (3) where the PHDs on the rings can tilt following changes in the geometry of lipid bilayer until the hemifission stage (4) is achieved. The PHD mobility is characterized by the tilt angle (α) between dynamin subunits assembled in adjacent rings. Although each PHD can tilt independently, we consider the mirror-symmetric tilt as the simplest approximation. Complete fission is stochastically coupled to disassembly of the metastable dynamin scaffold and is accelerated by membrane tension. **B.** The membrane wedging module of dynamin is formed by adjacent PHDs interacting with PI(4,5)P2 lipids (red) and inserting small hydrophobic regions into the lipid monolayer; the membrane wedging is approximated by a shallow hydrophobic inclusion (H_i) imposing stresses on the neighboring lipids (purple, see also Fig. S3). **C.** Dependence of the energy barrier (ΔW) between the constricted neck (3) and hemifission intermediate (4) on α (red) and H_i (black). The black curve was calculated assuming α as a free parameter, the energy barrier for H_i=0.7nm is indicated by the dashed line. The red curve was calculated using fixed H_i=0.7nm.